

# New challenges in beamline instrumentation for the ESRF Upgrade Programme Phase II

Jean Susini,\* Raymond Barrett, Joel Chavanne, Pablo Fajardo, Andy Götz, Jean-Luc Revol and Lin Zhang

European Synchrotron Radiation Facility, 71 avenue des Martyrs, 38000 Grenoble, France.

\*E-mail: susini@esrf.fr

Although beamline instrumentation is by nature driven by science, some recent examples serve as reminders that new technologies also enable new science. Indeed, exploiting the full scientific potential of forthcoming new storage rings with unprecedented source characteristics will, in many cases, require the development and implementation of novel instrumentation. In comparison with present synchrotron radiation facilities, the majority of beamlines should reap immediate performance benefits from the improved source emittance, principally through increased flux and/or horizontal beam size reduction at the sample. Instrumentation will have to develop along similar quantitative and qualitative trends. More speculative and more challenging is anticipating instrumentation that will be required by the new science made possible thanks to the unique coherence properties of diffraction-limited storage rings (DLSRs). ESRF has recently carried out a detailed feasibility study for a new ultra-low-emittance 6 GeV hybrid multibend storage ring, identified as ESRF Upgrade Programme Phase II. Although its performance is not expected to be equivalent to a DLSR source, the successful implementation of the ESRF Phase II project has to address scientific instrumentation issues that are also common to DLSRs. This article aims at providing a comprehensive review of some of the challenges encountered by the ESRF, in the context of the preparation of Phase II of its upgrade programme.

**Keywords:** ESRF upgrade; ultra-low emittance; heat-load optics; X-ray detectors; data management; synchrotron instrumentation.

© 2014 International Union of Crystallography

## 1. Introduction

Whereas most of the fundamental parameters of synchrotron radiation sources have been dramatically enhanced, progress in the reduction of the horizontal source emittance and associated increase of the transverse coherence are still too limited to open opportunities for truly new science. As an example, the very asymmetric source parameters translate into an inefficient use of the photons emitted in the horizontal plane by the source and represent an intrinsic limitation for many scientific applications of synchrotron radiation requiring high flux and/or high coherent brightness. Indeed, high space and time resolution in diffraction, spectroscopy and imaging would benefit from a more symmetric X-ray source with diffraction-limited performance in both the horizontal and vertical planes. Therefore, the emergence of concepts aiming at diffraction-limited storage rings (DLSRs) has triggered growing interest within the scientific community as they are expected to open a new era for the use of synchrotron light. However, to fully exploit the potential offered by this new class of synchrotron sources, a parallel effort will be necessary

for the development of beamline instrumentation. Although most of these developments are, by nature, science-driven and application-specific, all beamline designers will have to cope with more generic challenges such as transfer of brightness, coherence preservation, environmental stability, mechanical precision and volumes of data produced. This new paradigm is currently being addressed by the ESRF with the Phase II of its Upgrade Programme, in which a major upgrade of the ESRF storage ring has been proposed (ESRF, 2013*a*). This project anticipates a decrease in horizontal emittance by about a factor of 30 and a consequent increase in brilliance and coherence of the photon beam. The increase will be substantially higher than 30 at X-ray energies larger than 50 keV. In this context, the majority of the ESRF beamlines should reap immediate performance benefits from the improved source characteristics, principally through increased brightness and/or reduced horizontal beam size at the sample. Instrumentation will have to develop along similar quantitative and qualitative trends and another important component of this Upgrade Programme stands upon an ambitious instrumentation programme aiming at providing the entire beamline

portfolio with appropriate solutions adapted to the new source properties. Beamline instrumentation for specific applications are discussed in other science-related articles of this special issue of the *Journal of Synchrotron Radiation*, and so this article targets, in more general terms, some of the generic challenges to be addressed to fully exploit DLSRs by taking the ESRF's impending Upgrade Programme as a practical case. It does not aim to present an exhaustive picture of all the challenges associated with exploiting a DLSR but rather to illustrate with practical examples the expected evolution of the beamline instrumentation at the ESRF. Following a short description of the properties of the new ESRF photon source, this paper will discuss the problem of brightness transfer and associated heat-load management. Similarly, wavefront preservation will be touched upon briefly. The next section will be more speculative, providing a brief account of the main strategic lines of development being considered by the ESRF for the Upgrade Programme Phase II, concerning detectors and data management.

## 2. The new ESRF X-ray sources

A few years ago, as a contribution to a worldwide reflection on the feasibility of high-energy DLSRs, the ESRF explored several options for a new lattice design (Elleau & Ropert, 2003) that would be compatible with the existing infrastructure, thus minimizing costs. At that time, none of the preliminary designs were deemed suitable for further development, considered as too risky and too expensive, in particular regarding the challenges related to a reliable top-up injection and operation cost. Development in accelerator technologies during the last decades has led to many important advances featuring new magnet design, innovative vacuum technology, and revolutionary beam monitoring and orbit feedback systems. These new capabilities and technologies, today, provide a solid basis for the realisation of a substantially more advanced storage ring design (see numerous other articles throughout this issue of the *Journal of Synchrotron Radiation*) and in this context the ESRF Upgrade Programme now includes a new storage ring. The Phase II project, which is still in its definition phase, stands upon a new lattice based on a hybrid seven-bend achromat (HMB) which will replace the current double-bend achromat (DBA) based lattice. A full technical analysis of this concept is given elsewhere in this volume (Hettel *et al.*, 2014) and we recall briefly here the driving ideas. The HMB concept, with seven bends in the achromat cell, takes advantage of the large number of bending magnets

to reduce the horizontal emittance, as implemented in the MAX IV design, and sections with localized large dispersion to allow an efficient correction of chromaticity, as used in the classical DBA design. The proposed lattice produces a small emittance thanks to stronger focusing, softer bends and bends with quadrupole components. The design is severely constrained to fit within the existing infrastructure, conserving ring circumference, lattice periodicity and beamline positions. For bending-magnet sources, three-pole wigglers will be used to overcome the limitation induced by the lower bending magnet field of the new lattice. These short devices, inserted between two dipoles as optional source points, will provide and improve the photon flux in the hard X-ray region. The brilliance will also be significantly increased due to the smaller horizontal emittance and the reduced electron beam size in the vertical plane thanks to the smaller vertical beta function at the source. It is worth noting that for long-period wigglers (>150 mm) the source size is dominated by a depth-of-field effect and the light produced is essentially incoherent with a very limited gain in brilliance. While the equilibrium emittance of the current DBA is about 4.0 nm, the new lattice will reach an equilibrium emittance of 150 pm. In the vertical plane, the electron beam emittance will remain comparable with what is achieved presently (~5 pm) (Table 1). Since for hard X-rays the horizontal emittance of the photon beam is dominated by that of the electron beam, the brilliance from the different sources will be significantly enhanced (Fig. 1). Above 10 keV, the brilliance is increased by a factor higher than 26, while for lower photon energy the gain becomes smaller (factor of 18 at 1 keV) as the photon beam approaches the diffraction limit regime. Table 2 compares the perfor-

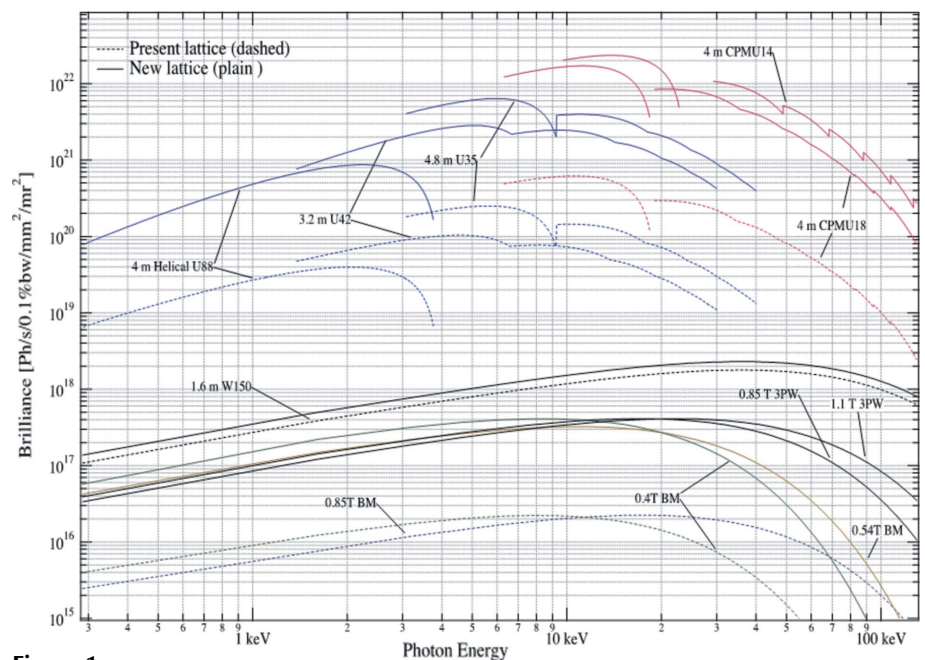


**Figure 1** Comparison of brilliance reached by different sources of the current and future ESRF lattices. The upper part corresponds to a number of undulators representative of the photon energy range covered by the ESRF [conventional devices operated with a minimum gap of 11 mm, short period small gap (5 mm) in-vacuum-type undulators such as cryogenic permanent-magnet undulators (CPMUs)].

**Table 1**

Comparison of the main parameters of the current and future ESRF storage rings.

	Current lattice	Future lattice
Lattice type	DBA	HMB
Circumference (m)	844.39	843.98
Energy (GeV)	6.04	6.00
Beam current (mA)	200	200
Natural emittance (pm)	4000	147
Energy spread (%)	0.106	0.095

**Table 2**

Comparison of the X-ray source parameters for current and future ESRF lattices in the case of a straight section equipped with a 4 m-long 18 mm-period undulator.

Energy	Lattice	RMS size ( $\mu\text{m}$ )		RMS divergence ( $\mu\text{rad}$ )	
		H	V	H	V
10 keV	Current low- $\beta$ section	49.8	6.2	105.6	5.1
	Current high- $\beta$ section	411.6	6.2	11.5	5.1
	New lattice	28.2	6.1	7.2	5.1
50 keV	Current low- $\beta$ section	49.6	4.4	105.5	4.5
	Current high- $\beta$ section	411.6	4.4	11.2	4.5
	New lattice	27.8	4.4	6.8	4.4

mances of the present and new lattice in terms of horizontal and vertical undulator source size and divergence for an 18 mm-period undulator (CPMU18). It must be recalled that, as indicated in Table 2, the ESRF is currently designed with alternating high-beta and low-beta cells with rather different beta functions (Ropert & Farvacque, 2006) exhibiting very different source parameters, whereas the new lattice will have relatively homogeneous parameters for all beamlines.

Transverse coherence is also a key feature of the new ESRF lattice since the coherent fraction depends on both photon source size and divergence. The reduction of the horizontal

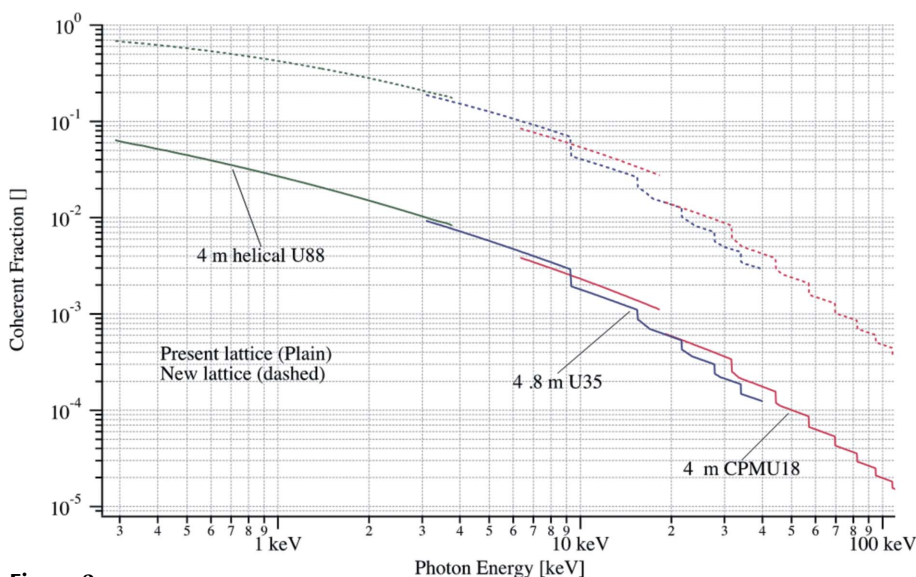


**Figure 2**

Comparison of the coherent fraction of the photon flux produced by different sources of the current and future ESRF lattices (for illustration, the full energy range is covered by three different insertion devices).

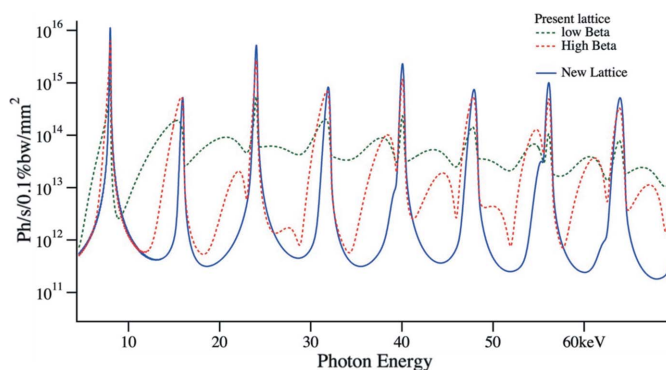


**Figure 3**

Spectral photon flux density (log scale) at 30 m from the source for a 4 m-long CPMU18 (gap 6 mm,  $K = 1.68$ ) for the present and new lattices.

emittance translates directly into an increased fraction of the photon flux from which the phase coherence is preserved transversally. The expected gain in coherent fraction exceeds one order of magnitude, and is logically the same as gain in brilliance. Fig. 2 shows the coherent fraction of the photon flux achieved with the existing and new lattice for the CPMU18 undulator.

### 3. Beam transport systems

The fundamental roles of the beam transport and conditioning systems are to transfer the photon beam from the front-end down to the experimental hutch(es) and to tailor the X-ray beam properties prior to delivery to the end-stations. In this respect such systems may be required to act upon beam size, beam divergence, photon flux, temporal and/or spatial coherence, and polarization. An important and related role of these systems for an ultra-low-emittance source is to modulate the unwanted power developed by the source in order to

alleviate thermal deformation or radiation damage of downstream components or samples, while preserving brightness and coherence.

#### 3.1. Brightness transfer and power management

The on-axis photon flux density reaching the first optical component in a beamline is largely dominated by the divergence of the source. Therefore, in comparison with present performances, one can expect a moderate gain (about a factor of two) in flux for high-beta beamlines while low-beta beamlines will benefit from a much higher flux than at present (about one order of magnitude). As illustrated in Fig. 3, which compares the spectral photon flux density at 30 m from the source generated by a 4 m-long CPMU18 (gap 6 mm,  $K = 1.68$ ) for the current and new lattices, the decrease of

**Table 3**

Comparison of the X-ray source parameters for current and future ESRF lattices in the case of a straight section equipped with a 4 m-long 18 mm-period undulator at 10 keV.

The integrated power refers to the total power integrated over a surface equal to the RMS beam size.

Lattice	RMS photon beam size at 30 m ( $\mu\text{m}$ )		Integrated power (W)	Integrated power in 0.1% bandwidth (W)
	H	V		
Low $\beta$	3100	150	180	0.77
High $\beta$	530	150	42	0.77
New lattice	220	150	17	0.77

source emittance translates into a much higher spectral purity of the undulator harmonics. As discussed hereafter, both spectral purity and beam profile will have implications on the heat load of the optical components.

So far, for typical ESRF beamlines, the monochromatic component of the white beam corresponds to a very small fraction of the total incident power which is eliminated at the first optical components. In general terms, for an undulator source, the spatial distribution of the power density is primarily driven by the deflection parameter  $K$  of the undulator. For a planar vertical field undulator (the vast majority of ESRF undulators), the horizontal angular distribution of the power density has a typical width (RMS) of  $K/\gamma$  with  $\gamma$  the relativistic Lorentz factor. In the vertical direction, this width is  $1/\gamma$ , and as a result the spatial distribution of the power density has a weak dependence upon the horizontal electron beam emittance. The total power generated by standard insertion devices in the new lattice will be identical to the power emitted today by the same devices, and power densities will be very comparable with those currently experienced on the high-beta sources (Fig. 4). However, in practice the incoming beam is collimated with a dedicated aperture (front-end and primary slits) to cut off the unwanted power. The size of this aperture matches usually the size of the beam corresponding to the central cone emitted by the undulator at a given photon energy. Table 3 presents the horizontal and vertical RMS size of a 10 keV monochromatic beam at 30 m

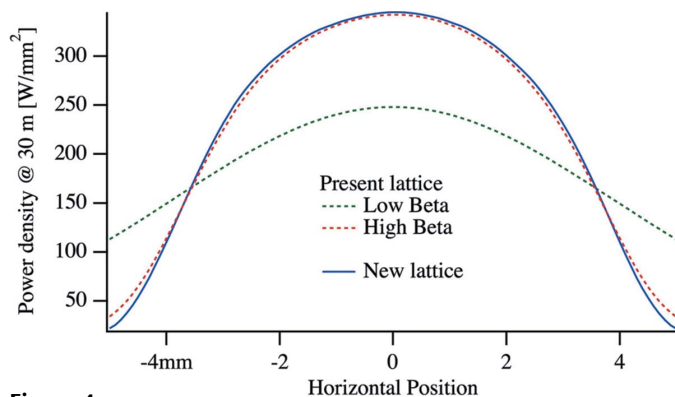


**Figure 4** Horizontal profile of the power density integrated over the full undulator spectrum (white beam) at 30 m from the source (4 m CPMU18) for the present and new lattices.

from the undulator source and the integrated power through an aperture of that particular size (expressed as  $1\sigma$ ). This table illustrates that the most marked improvements in the source quality will be derived from the considerable reduction of the horizontal emittance. The consequent narrowing ( $\sim 1.5\times$ ) of the undulator energy peak profiles will allow more flux to be accepted into the bandpass of typical monochromating optics. As shown in Table 3, for the same monochromatic power (0.77 W within 0.1% bandwidth) at 10 keV, the first optical component will be exposed to a total power of only 17 W compared with 42 W and 180 W for the high-beta and low-beta current beamlines, respectively. Similar results can be derived at higher photon energies. This example outlines that, regarding the ‘useful’ photon flux, ultra-low-emittance sources are much more ‘efficient’. Consequently, through careful optical design and component optimization, power management aspects should not be a limit to the ability to exploit the source to its full potential. Initial calculations indicate that the thermal management solutions which are currently deployed should remain applicable in their present or slightly adapted form in most cases. For ‘passive’ components (*e.g.* windows, slits, filters, apertures, choppers...), on the basis of cooling considerations alone, the current designs should be appropriate for use with the new source. For more sensitive optical systems (*e.g.* mirrors, monochromators, lenses), this extrapolation is not straightforward. On one hand, total power will be lower and power density remains within a very manageable range but on the other hand the power density profile and the illumination geometry are important parameters in the optimization of the cooling strategy. Today, the most advanced designs of optics cooling include for optimization of the optics geometry (dimension and cross section) and illumination geometry as a function of the power distribution (Zhang *et al.*, 2013, 2014; Khounsary, 1999). This optimization will be more challenging with sharper undulator peaks. Fig. 5 shows the power distribution, for a low-beta source, produced by a 32 mm-period undulator (1.6 m long) for two gap values corresponding to first harmonic energy of 4 and 8.5 keV. It depicts the very different power distributions for the new and present lattices, particularly in the horizontal plane where the spatial power distribution is much sharper, inducing much stronger thermal gradients for horizontally deflecting optics. This is illustrated in Fig. 6, which shows the residual RMS slope error induced by thermal load for a horizontally deflecting mirror exposed to power densities as displayed in Fig. 5. It compares the slope error as a function of the groove depth,  $W_{\text{cut}}$ , for the new and present lattices. This side groove, used in combination with a side-cooling configuration, acts as a thermal choke which reduces the temperature gradients developed at the sensitive optical surface. For the current configuration,  $W_{\text{cut}}$  can be optimized to prevent thermal deformation over the full energy range while the power density increases by a factor of five when closing the gap. On the contrary, with the new lattice, for the same configuration the power density increases by a factor of only two but the  $W_{\text{cut}}$  optimization does not prevent a residual deformation and cannot be optimized for the entire energy range. This example

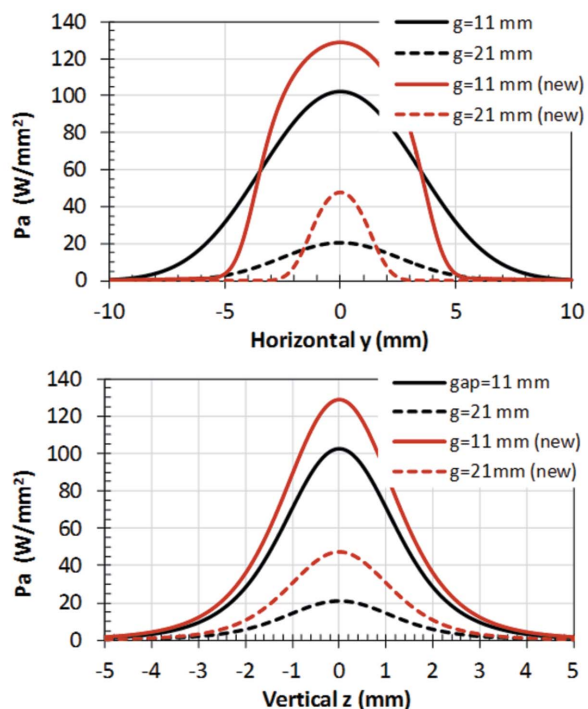


**Figure 5** Horizontal and vertical profiles of the power density for two gap values of a 1.6 m-long, 32 mm-period linear undulator, corresponding to energies of the first harmonic of 4 and 8.5 keV, at 30 m from the source, for the present lattice (low-beta case) and the new lattice.

highlights that in terms of cooling optimization the peak power is less problematic than the power distribution. Furthermore, it is notable that in all cases the slope error induced by thermal deformation remains very low compared with other potential sources of figure distortion (polishing, mechanical clamping...).

### 3.2. Wavefront preservation and characterization

One of the primary scientific driving forces pushing the development of DLSRs and XFELs is the production and

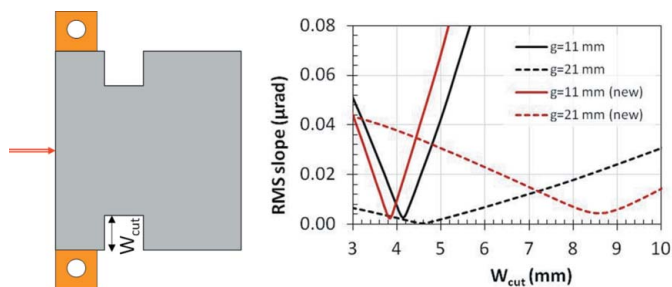


**Figure 6** Schematic cross section (left) of an optimized cooling geometry for a white-beam mirror. The mirror is depicted in a horizontally deflecting geometry with the beam impinging onto the optical surface (red arrow) with the beam direction into the page. Side-mounted water-cooled heat exchangers (orange) are placed close to the optical surface in combination with notches along the side-faces of the mirror. Optimization of the depth of the groove ( $W_{cut}$ ) allows thermal deformation of the optical surface to be minimized. The graph shows the dependence of the thermally induced slope error upon the groove depth, for power distributions computed in Fig. 5.

exploitation of highly (if not fully) transversally coherent X-ray beams. The ESRF project is expected to foster coherent-based techniques in the hard X-ray domain. As shown in Fig. 2, the reduction of the horizontal emittance translates directly into a substantial increase of the fraction of the transverse coherence of the X-ray beam at energies exceeding 30 keV. For applications exploiting the coherent illumination, such as diffraction-limited focusing, coherent imaging and coherent scattering, it will be then crucial to ensure an optimal transfer of this coherence down to the sample. XFEL projects fostered significant technological advances in design and production of beamline systems with improved performances (Geloni *et al.*, 2010; Boutet & Williams, 2010; Tono *et al.*, 2013), and the last decade has seen significant efforts to find engineering solutions to design and produce speckle-free components (Yabashi *et al.*, 2014). Although performances of beryllium windows, diamond-based absorbers, mirrors and monochromators and in-line beam position monitors have seen dramatic progress regarding their impact on wavefront fidelity, further efforts are still needed to reach near-perfect wavefront propagation. Moreover, maintaining the optimal performance of optics over long periods [*e.g.* avoiding degradation by surface contamination phenomena (SOLEIL, 2012)] is challenging even for high-energy applications. ESRF is considering three main lines of development to meet this objective:

*Optics manufacturing.* For the typical hard X-ray wavelengths employed at the ESRF, application of the Maréchal criterion (Hignette *et al.*, 2001) indicates figure error requirements for reflective optics in the sub-1 nm range. Nevertheless, in many apparently less-demanding applications there is significant incentive to reduce the slope and figure errors to the sub-0.1  $\mu\text{rad}$  RMS and sub-1 nm peak-to-valley scale in order to reduce the contrast of the intensity inhomogeneities which are typically observed in the reflected beams from mirrors in either unfocused or defocused beams. As an example, Fig. 7 shows such features arising from a partially multilayer-coated sub- $\text{\AA}$  RMS microroughness Si

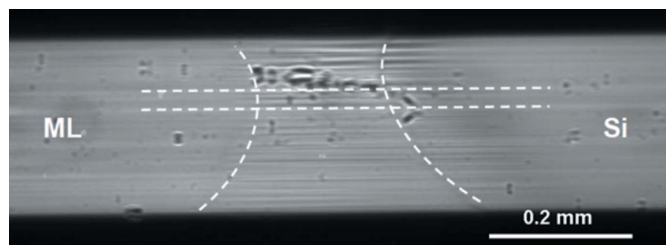


**Figure 7** Flat-field image of a partially multilayer coated Si substrate recorded in total reflection conditions (projected  $q$ -vector vertical) with monochromatic illumination (15 keV). The region between the curved vertical dashed lines indicates the transition zone between the multilayer (ML) coating (left) and the uncoated Si substrate (right). Continuity of line features across the coating edge (the horizontal dashed lines show two such examples) illustrate the predominant influence of the substrate on wavefront degradation. The image is foreshortened in the vertical direction due to the grazing incidence ( $0.12^\circ$ ) illumination and intensity corrected to eliminate any intensity fluctuations due to the incoming illumination or detector response.

substrate with  $<1 \text{ \AA}$  RMS microroughness, indicating that currently such inhomogeneities are dominated by the mid-range spatial frequency slope and figure errors of the underlying substrate (Morawe *et al.*, 2013). Whilst the manufacture of high-quality substrates is essentially the preserve of industrial suppliers, the ESRF plans to explore corrective figuring methods by subtractive [*e.g.* ion beam figuring (Peverini *et al.*, 2010; Preda *et al.*, 2013)] or additive [*e.g.* differential deposition (Alcock & Cockerton, 2010)] techniques as well as mechanical correction techniques (Nicolas *et al.*, 2013). Improvements in both refractive and diffractive lens fabrication are also necessary to enhance their performance (particularly with regard to efficiency, apertures and parasitic scattering) and will yield benefits in current applications and extend their use in other fields.

*On-line and qualification metrology methods.* Similarly, the development of new metrology tools will be crucial to qualify optics and validate new manufacturing techniques. Coupling manufacturing and metrology into a single process is expected to be the most promising strategy. When considering coherence preservation, at-wavelength metrology will be necessary and the ESRF is exploring several X-ray-based methods (Berujon *et al.*, 2012; Berujon & Ziegler, 2012). Similarly, diffraction imaging techniques (*e.g.* topography, Talbot imaging) remain powerful diagnostic tools for optical quality (Kluender *et al.*, 2009).

*Modelling.* Modelling, simulation and optimization tools will be paramount for the optimal exploitation of the source. As an ultimate aim, the tools to be developed for optical design should permit flexible choice of the optical interactions to be modelled *via* a common interface using, according to the specific requirements, fully incoherent, partially coherent or fully coherent illumination. While a number of codes exist for the source, there are few mature codes for the simulation of partially coherent wavefronts propagating through complex systems of real optical components (Morawe *et al.*, 2008; Osterhoff *et al.*, 2013; Chubar *et al.*, 2011). The implementation of freeform optical surfaces and the straightforward consideration of manufacturing errors into the tools is essential. Global optimization methods and codes, *e.g.* for the optimization of refractive-lens-based systems and bent crystal optics, should be incorporated into the toolboxes. Straightforward transfer of results from mechanical, dynamic and thermal modelling, and metrology measurements to optical simulation codes is essential to facilitate iterative optimization studies.

### 3.3. Optics development and opportunities for new optical schemes

Huge progress has been made in the quality of X-ray optics and their implementation since the advent of third-generation synchrotron sources. Nevertheless, continual improvements in source characteristics have meant that often the optical systems continue to limit the beamline performance. Significant improvement of the underlying X-ray optics technologies is necessary to allow optimal exploitation of DLSRs. A comprehensive review of the anticipated future needs for

X-ray optics developments has recently been published by the US DoE (Mills & Padmore, 2013). As already stated, the proposed new ESRF source will produce very sharp undulator harmonics and less asymmetric beam. The new beam parameters will offer opportunities to exploit new concepts for low-loss beam transport and conditioning systems based on on-axis optics such as rotationally symmetric lenses. Taking advantage of the substantially reduced horizontal source size and the beam divergence, these new systems integrated into the front-end could transfer the photon beam almost without losses from the front-end to any further secondary optical systems (mirrors, crystals, lenses, *etc.*) or directly to the end stations. For example, with the reduction in the undulator harmonic energy-width, the use of the strong dispersion properties of refractive lenses in combination with an energy-selecting aperture placed at the achromatic focal point may offer an effective method to create a high-throughput broadband monochromator (Polikarpov *et al.*, 2014). This development would be a logical step after the successful implementation of transfocators (Vaughan *et al.*, 2011), which are tunable devices based on refractive lenses. Since 2007, a large variety of transfocators and lens changers were installed on half of the ESRF beamlines. This scheme might have advantages in filtering out the unwanted power developed by the source in order to alleviate thermal deformation or radiation damage of downstream optical components such as mirrors and crystals. The pre-focused or collimated beams with smaller sizes/footprints might significantly reduce the length of mirrors and crystals. It is worth noting that, in order to install transfocators into front-ends, the lens assembly must be capable of sustaining a high power density, provide alignment capabilities and feature exceptional reliability. For all but the soft X-ray regime, where single particle photon emission divergence dominates the beam size, the reduced horizontal emittance of the Phase II storage ring source leads to a typical reduction in the aperture size (for equivalent flux), ranging from 30% (3 keV) to 65% (100 keV). For mirror optics this translates either to a reduced useful mirror length or improved flux collection following the lattice upgrade. For the former case, this offers the possibility for more compact and higher stability systems coupled with the improvements in the optical quality (slope and figure errors) achievable for shorter optics. For lens-based systems the reduced beam size will overcome some of the aperture limitations and might allow them to replace, advantageously, mirror systems in some focusing applications.

### 4. Two other major challenges for scientific instrumentation

Most of the new applications which are foreseen with DLSRs, and also included in the scientific case of the ESRF Phase II upgrade programme, stand upon the brightness increase and the dramatic enhancement of the transverse horizontal coherence of the beam, in particular at high energies (more than a factor of 40). Science-wise, it can be anticipated that in very general terms these new source performances will

translate into the growing use of nano-beams and a wider deployment of coherence-based techniques. Furthermore, experiments limited by radiation damage may benefit from moving towards high energies and/or performing experiments faster. Enabling technologies will have to be further developed to make possible the foreseen scientific opportunities. The ESRF is currently defining its instrumentation roadmap to adapt the existing beamline portfolio to the full potential of the ESRF source. The two main components of this development plan are presented below.

### 4.1. Detection challenges for the ESRF Upgrade

Because constructing an *ideal* and universal X-ray detector has thus far proved impossible, in practice a diversity of detection technologies and concepts need to be deployed, each satisfying a particular set of requirements that are critical for a family of applications. Nevertheless, given the cost and timescales involved, developing a completely new detector system for each individual application is obviously not a viable approach. The ESRF has palliated this fact by focusing on certain key hardware and software components and strengthening its in-house capabilities for integrating and customizing complete detector systems (Martin & Koch, 2006; Ponchut *et al.*, 2011; Labiche *et al.*, 2007). The example in Fig. 8 illustrates this approach. However, the increase of beam intensity and the foreseen boost of coherent diffraction techniques that will be brought by the new Phase II source will significantly impact the requirements for future components and systems. In terms of detectors, the possibility of reaching shorter timescales with similar photon statistics or shifting the energy range of certain experimental techniques towards

higher hard X-rays will require the development of a new generation of advanced detector components and technologies. The following sections present succinctly some of these challenges, the views from the ESRF and some relevant implications.

**4.1.1. Management of higher photon fluxes and shorter exposure times.** The increase in effective photon flux of the Phase II source will require detectors with extended dynamic range that are also able to cope with shorter timescales. This is expected to be particularly true for diffraction and scattering techniques, often implemented at low-beta beamlines today, for which current photon-counting pixel detectors such as PILATUS, MAXIPIX, XPAD or EIGER will be severely challenged. Boosting the maximum photon rate of two-dimensional counting detectors would require novel technologies that include some level of signal amplification built into the X-ray sensors (Fajardo *et al.*, 2013). However, because such technologies are still rather immature, many experiments are expected to rely on high-sensitivity charge-integrating devices instead of photon-counting. Applications at medium energies up to 20 keV will profit from ongoing and future developments of silicon-based, integrating, hybrid pixel detectors for free-electron lasers (Mozzanica *et al.*, 2014). The implementation of integrating pixel detectors, equipped with high-Z semiconductor sensors such as CdTe or GaAs for higher-energy X-rays above 30 keV, will be particularly challenging as those devices are more sensitive to material inhomogeneities and imperfections than their photon-counting counterparts. This is one of the reasons why indirect detection devices based on X-ray-to-light converters are still expected to play an important role in the future for very high energies. In this sense the continuous progress of scientific quality CMOS imaging sensors (Spivak *et al.*, 2009; Turchetta *et al.*, 2011) makes indirect detection schemes based on this technology an attractive and cost-effective option. The achievable performance of future advanced integrating detectors for high energies will be determined, to a large extent, by actual progress made on the quality and properties of new sensor materials with high stopping power, be it semiconductors (Owens & Peacock, 2004) or scintillators (Derenzo *et al.*, 2003; Nikl, 2006).

Increased flux will result in a substantial reduction of the total time required to perform a complete sample scan, which promotes the application of fast mapping techniques. The detectors will have to operate with one or two orders of magnitude shorter readout times and at correspondingly increased frame rates to not spoil the efficiency of experiments. The new source will also open new scientific opportunities for experiments in the micro- and sub-microsecond range and this will require pushing the time resolution of the detectors to values limited only by the available photons. In that range the ultimate time resolution of two-dimensional detectors will not be reached by a brute force approach based merely on increasing their frame rate; it will require *ad hoc* readout schemes that should be adapted to the specificities of the target experiments. Such schemes could be based, for instance, on event-by-event (also called sparse or list mode

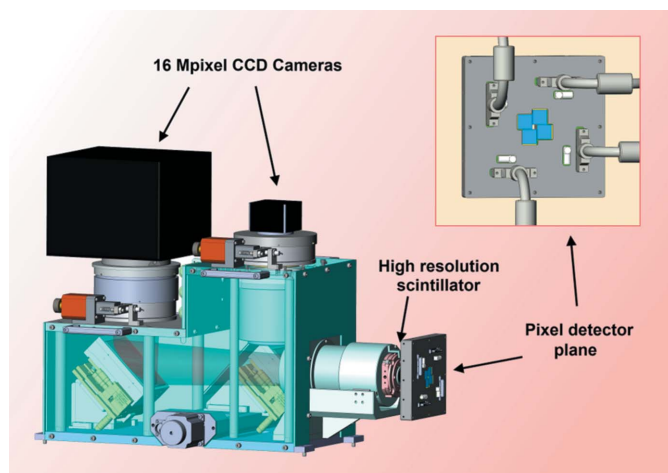


**Figure 8**

Advanced composite detector built for the ESRF nanoprobe (ID16A). The detector has been designed for X-ray imaging and ptychography applications and integrates two indirect detection imaging cameras and a pixel detector based detection plane to collect the higher- $q$  coherent scattering. The instrument includes both generic and modified ESRF components such as high spatial resolution scintillators, full custom design lenses, a 16 Mpixel FReLoN camera and four special Maxipix modules.

readout) or on local storage of the images at the detector front-end, as is already implemented in some detectors under development for the European XFEL (Sztuk-Dambietz *et al.*, 2013).

**4.1.2. Reaching higher spatial resolution for single-photon sensitive detectors.** A sufficient detection angular resolution is mandatory for all experiments with coherent beams. The same is true for most of the high-resolution wavelength-dispersive spectrometers at the ESRF using one-dimensional or two-dimensional detectors. In both families of experiments, single-photon sensitivity is crucial to produce noise-free data. The Phase II source will accentuate the angular resolution requirements of detectors due to the ability to coherently illuminate samples of larger size and the completely new possibility of applying coherent beam techniques at shorter photon wavelengths in order to image samples inside absorbing environments such as high-pressure cells. Although the angular resolution in coherent scattering applications can, in principle, be improved by moving the detector away from the sample, in practice some experiments today are already limited by the minimum pixel size of the existing detectors. This is particularly the case in experiments in which the maximum sample-to-detector distance is limited. In Phase II, the practical ability of extending coherent beam techniques in optimum conditions to a diversity of scientific cases, experimental set-ups and higher photon energies will depend crucially on the availability of efficient and sensitive two-dimensional detectors with spatial resolutions beyond 55  $\mu\text{m}$ , the minimum pixel size of current photon-counting area detectors. Although hybrid pixel detectors in photon-counting or integrating mode are excellent candidates to achieve high sensitivity and noise-free operation, reducing the pixel size is challenging due to the intrinsic spatial resolution limitations of the X-ray sensors (Dinapoli *et al.*, 2014). Reaching good spatial resolution and very small pixels is far from trivial and involves a certain level of signal processing for photon position refinement (Schubert *et al.*, 2012). In addition, keeping acceptable photon detection rates would require implementing part of the processing logic inside the pixel electronics.

**4.1.3. Improvement of detection efficiency.** As a high-energy source, increasing detection efficiency for hard X-rays at the ESRF is a long-standing and relatively elusive challenge. The relevance and importance of this objective will have to be further reinforced with the new source. The increased brilliance of the source and transversal coherence of the future beams over the whole spectral range will make possible experiments with very hard X-rays that today are restricted to lower photon energies. Pushing the working energy to higher values may provide crucial benefits, as important as substantially reducing the radiation damage of fragile and sensitive samples or allowing new experimental techniques in complex environments. Unfortunately, detection of X-rays above 20 keV in most cases suffers from very severe efficiency limitations that worsen very rapidly as photon energy increases. This is illustrated in Fig. 9, which presents the absorption of various high-density X-ray sensor materials,

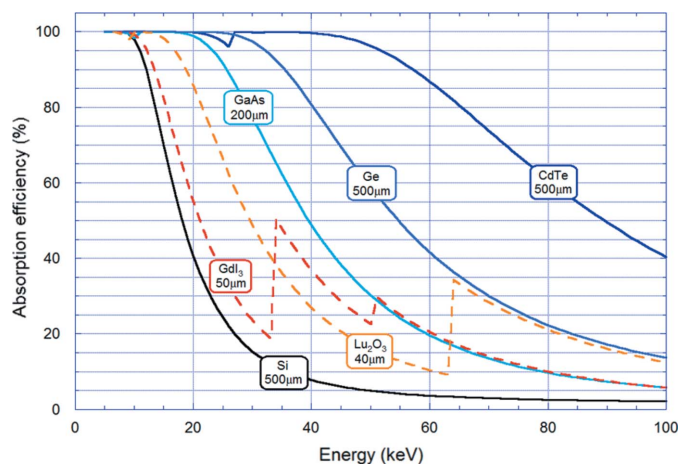


**Figure 9**

Absorption efficiency calculated for various high stopping power X-ray sensor materials. The figure shows how high-Z semiconductors (GaAs, Ge, CdTe, in solid lines) and high density scintillators (GdI<sub>3</sub>, Lu<sub>2</sub>O<sub>3</sub>, in broken lines) compare with 500  $\mu\text{m}$ -thick silicon, typically used in pixel detectors today.

both semiconductors and scintillators, compared with a typical 500  $\mu\text{m}$ -thick silicon sensor, whose low absorption makes it unsuitable in that energy range. The problem of weak absorption efficiency is aggravated when aiming at reaching high spatial resolution as the sensor must be kept thin enough to preserve the lateral resolution.

## 4.2. Big data challenges

The ESRF (ESRF, 2013b) and synchrotrons in general have been generators of 'big data' for a number of years now (Berkowitz, 2013) and this will only become more challenging in the future. For instance, in 2013 the average ESRF data production stood at 2.5 TB per day. This number is only an average number and hides the fact that the majority of big data are produced by a subset of the beamlines and are technique specific. This is, however, changing rapidly due to the generalization of techniques, the development of new experimental techniques and improved detectors. In the future more and more beamlines will produce big data. For example, new two-dimensional detectors are capable of generating images of 12 Mbytes at a rate of 750 images per second (*e.g.* Eiger 4M). This corresponds to an internal data rate of 9 GB s<sup>-1</sup>. Even assuming a duty cycle as low as 1% (*i.e.* 15 min per day), such a detector would still produce 1 TB per day of compressed data. New techniques based on scanning microscopy today produce 1 TB in a few hours (Chahine *et al.*, 2014) and are capable of producing 10 TB per day if only the computing infrastructure could support it. The main limitation is having the necessary computing infrastructure in place to manage such large volumes of data during and after the experiment. The computing infrastructure includes the data acquisition, storage, analysis and exporting collectively referred to as data management. The data management infrastructure is heavily challenged by the ever-increasing data volumes. Current solutions need to be re-thought in order to

solve the challenges to be faced in the near future with huge volumes of data. Part of the solution is to provide more and more dedicated storage buffers to collect the incoming data without loss (Fig. 10). Data formats are being optimized to produce bigger files (based on HDF5), metadata are being stored in databases to make them searchable and immediately available for data analysis, and dedicated massively parallel compute power is being provided to speed up the data analysis to provide online feedback on the quality of the data. In addition, the file systems and data backup solutions have to be scaled up to handle the increased data rates and volumes.

Managing the data and providing dedicated computing power is only part of the solution; the data also need to be analysed. Data analysis software has to be developed and pipelines provided so that users can analyse their data during and after the experiment. Big data increasingly means: data too big to export to the user's home institute due to limited bandwidth and slow export media. Users often do not have adequate resources to manage and analyse big data in their home institutes. This means that keeping data at or close to the source and providing users with an efficient remote interaction with their data is becoming a necessity. In this case data analysis runs on the computing infrastructure of the source institute. Combined with the fact that more and more users need help to analyse their data in order to get the best out of them, the next step is to provide data analysis as a service to users. In the future the efficient use of synchrotrons will depend critically on data management and on providing data analysis as a service.

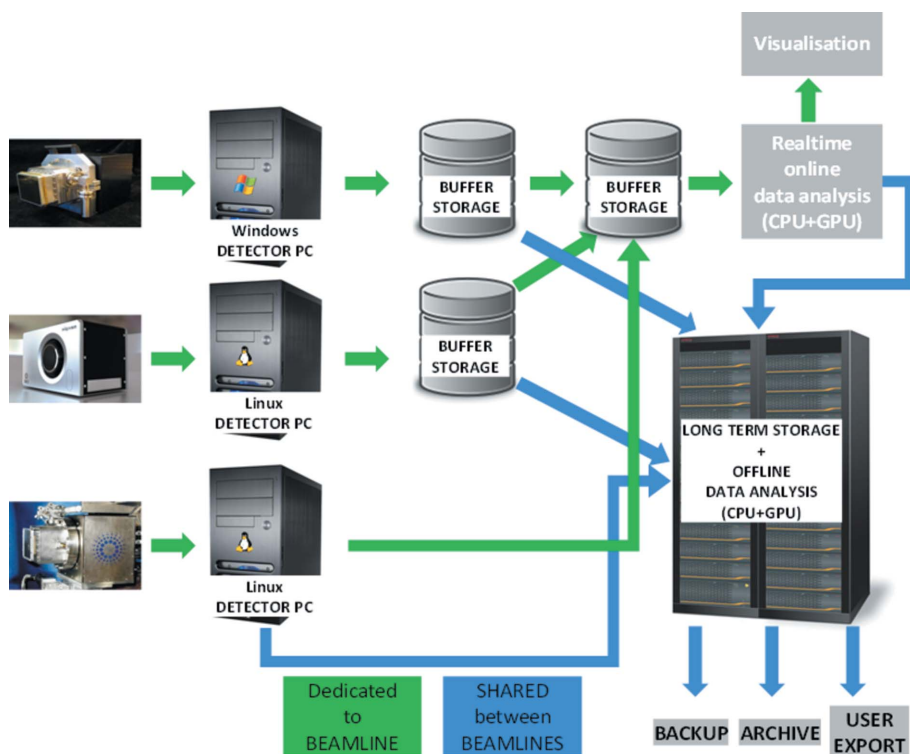


**Figure 10**  
Schematic of ESRF solution for a beamline using several two-dimensional detectors with different detector types. It relies on dedicated network links, computer resources and storage for multiple high-speed detectors.

## 5. Conclusion and outlook

The ultra-low-emittance storage rings are expected to open a new era in X-ray photon science on the condition that scientific instrumentation can be developed at the level needed to fully exploit the source properties. The ESRF Phase II upgrade stands perfectly in this paradigm, and this article aimed at providing insight into the most challenging elements of the ESRF instrumentation roadmap. It primarily includes heat-load management, coherence preservation, new detectors and solutions to anticipate the data deluge associated with the new capacities of new beamlines. All these challenges will require a significant engineering effort, but are common with all future DLSRs. The ESRF project will provide an ideal context to explore and validate engineering solutions in a collaborative framework with other similar projects.

The instrumentation roadmap of the ESRF Upgrade Programme involved a large number of ESRF colleagues and the authors wish to thank them all for their valuable contributions. In particular, we wish to thank P. Raimondi, H. Reichert, Y. Dabin, R. Dimper and A. Snigirev for fruitful discussions.

## References

Alcock, S. G. & Cockerton, S. (2010). *Nucl. Instrum. Methods Phys. Res. A*, **616**, 110–114.  
 Berkowitz, J. (2013). *DEIXIS Mag.* **13**, 20–27.  
 Berujon, S., Wang, H. C., Ziegler, E. & Sawhney, K. (2012). *AIP Conf. Proc.* **1466**, 217–222.  
 Berujon, S. & Ziegler, E. (2012). *Opt. Lett.* **37**, 4464–4466.  
 Boutet, S. & Williams, G. J. (2010). *New J. Phys.* **12**, 035024.  
 Chahine, G. A., Richard, M.-I., Homs-Regajo, R. A., Tran-Caliste, T. N., Carbone, D., Jacques, V. L. R., Grifone, R., Boescke, P., Katzer, J., Costina, I., Djazouli, H., Schroeder, T. & Schüllli, T. U. (2014). *J. Appl. Cryst.* **47**, 762–769.  
 Chubar, O., Berman, L., Chu, Y. S., Fluorasu, A., Hulbert, S., Idir, M., Kaznatcheev, K., Shapiro, D., Shen, Q. & Baltser, J. (2011). *Proc. SPIE*, **8141**, 814107.  
 Derenzo, S. E., Weber, M. J., Bourret-Courchesne, E. & Klintonberg, M. K. (2003). *Nucl. Instrum. Methods Phys. Res. A*, **505**, 111–117.  
 Dinapoli, R., Bergamaschi, A., Cartier, S., Greiffenberg, D., Johnson, I., Jungmann, J. H., Mezza, D., Mozzanica, A., Schmitt, B., Shi, X. & Tinti, G. (2014). *J. Instrum.* **9**, C05015.  
 Elleaume, P. & Ropert, A. (2003). *Nucl. Instrum. Methods Phys. Res. A*, **500**, 18–24.  
 ESRF (2013a). *ESRF Upgrade Programme Phase II (2015–2019) White Paper*, <http://www.esrf.eu/files/live/sites/www/files/about/upgrade/documentation/white-paper-upgrade-phaseII.pdf>.  
 ESRF (2013b). *ESRF Newsl.* **65**, 1–26.  
 Fajardo, P., Baron, A. Q. R., Dautet, H., Davies, M., Fischer, P., Göttlicher, P.,

- Graafsma, H., Hervé, C., Rüffer, R. & Thil, C. (2013). *J. Phys. Conf. Ser.* **425**, 62005–62008.
- Geloni, G., Saldin, E., Samoylova, L., Schneidmiller, E., Sinn, H., Tschentscher, T. & Yurkov, M. (2010). *New J. Phys.* **12**, 035021.
- Hettel, R. (2014). *J. Synchrotron Rad.* **21**, 843–855.
- Hignette, O., Peffen, C., Alvaro, V., Chinchio, E. & Freund, A. K. (2001). *Proc. SPIE*, **4501**, 43–53.
- Khounsary, A. M. (1999). *Proc. SPIE*, **3773**, 78–87.
- Kluender, R., Masiello, F., van Vaerenbergh, P. & Härtwig, J. (2009). *Phys. Status Solidi A*, **206**, 1842–1845.
- Labiche, J. C., Mathon, O., Pascarelli, S., Newton, M. A., Ferre, G. G., Curfs, C., Vaughan, G., Homs, A. & Carreiras, D. F. (2007). *Rev. Sci. Instrum.* **78**, 091301.
- Martin, T. & Koch, A. (2006). *J. Synchrotron Rad.* **13**, 180–194.
- Mills, D. & Padmore, H. (2013). *X-ray Optics for BES Light Source Facilities*, [http://science.energy.gov/~media/bes/pdf/reports/files/BES\\_XRay\\_Optics\\_rpt.pdf](http://science.energy.gov/~media/bes/pdf/reports/files/BES_XRay_Optics_rpt.pdf).
- Morawe, C., Barrett, R., Friedrich, K., Klünder, R. & Vivo, A. (2013). *J. Phys. Conf. Ser.* **425**, 052027.
- Morawe, Ch, Guigay, J. P., Mocella, V. & Ferrero, C. (2008). *Opt. Express*, **16**, 16138–16150.
- Mozzanica, A., Bergamaschi, A., Cartier, S., Dinapoli, R., Greiffenberg, D., Johnson, I., Jungmann, J., Maliakal, D., Mezza, D., Ruder, C., Schaedler, L., Schmitt, B., Shi, X. & Tinti, G. (2014). *J. Instrum.* **9**, C05010.
- Nicolas, J., Ruget, C., Juanhuix, J., Benach, J. & Ferrer, S. (2013). *J. Phys. Conf. Ser.* **425**, 052016.
- Nikl, M. (2006). *Meas. Sci. Technol.* **17**, R37–R54.
- Osterhoff, M., Morawe, C., Ferrero, C. & Guigay, J. P. (2013). *Opt. Lett.* **38**, 5126–5129.
- Owens, A. & Peacock, A. (2004). *Nucl. Instrum. Methods Phys. Res. A*, **531**, 18–37.
- Peverini, L., Kozhevnikov, I. V., Rommeveaux, A., Vaerenbergh, P. V., Claustre, L., Guillet, S., Massonnat, J. Y., Ziegler, E. & Susini, J. (2010). *Nucl. Instrum. Methods Phys. Res. A*, **616**, 115–118.
- Polikarpov, M., Snigireva, I. & Snigirev, A. (2014). *J. Synchrotron Rad.* **21**, 484–487.
- Ponchut, C., Rigal, J. M., Clément, J., Papillon, E., Homs, A. & Petitdemange, S. (2011). *J. Instrum.* **6**, C01069.
- Preda, I., Vivo, A., Demarcq, F., Berujon, S., Susini, J. & Ziegler, E. (2013). *Nucl. Instrum. Methods Phys. Res. A*, **710**, 98–100.
- Roport, A. & Farvacque, L. (2006). *Proceedings of EPAC 2006*, Edinburgh, Scotland. p. 1942.
- Schubert, A., Bergamaschi, A., David, C., Dinapoli, R., Elbracht-Leong, S., Gorelick, S., Graafsma, H., Henrich, B., Johnson, I., Lohmann, M., Mozzanica, A., Radicci, V., Rassool, R., Schädler, L., Schmitt, B., Shi, X. & Sobott, B. (2012). *J. Synchrotron Rad.* **19**, 359–365.
- SOLEIL (2012). *SRI2012 Satellite Workshop: Carbon Contamination of Optics, Causes, Characterisation and in situ Treatments*, 16 July 2012, <http://www.synchrotron-soleil.fr/portal/page/portal/Soleil/ToutesActualites/Workshops/2012/SRI2012-Sat.Carbon12/Program>.
- Spivak, A., Belenky, A., Fish, A. & Yadid-Pecht, O. (2009). *IEEE Trans. Electron Dev.* **56**, 2446–2461.
- Sztuk-Dambietz, J., Hauf, S., Koch, A., Kuster, M. & Turcato, M. (2013). *Proc. SPIE*, **8778**, 87780U.
- Tono, K., Togashi, T., Inubushi, Y., Sato, T., Katayama, T., Ogawa, K., Ohashi, H., Kimura, H., Takahashi, S., Takeshita, K., Tomizawa, H., Goto, S., Ishikawa, T. & Yabashi, M. (2013). *New J. Phys.* **15**, 083035.
- Turchetta, R., Guerrini, N. & Sedgwick, I. (2011). *J. Instrum.* **6**, C01099.
- Vaughan, G. B. M., Wright, J. P., Bytchkov, A., Rossat, M., Gleyzolle, H., Snigireva, I. & Snigirev, A. (2011). *J. Synchrotron Rad.* **18**, 125–133.
- Yabashi, M., Tono, K., Mimura, H., Matsuyama, S., Yamauchi, K., Tanaka, T., Tanaka, H., Tamasaku, K., Ohashi, H., Goto, S. & Ishikawa, T. (2014). *J. Synchrotron Rad.* **21**, 976–985.
- Zhang, L., Barrett, R., Cloetens, P., Detlefs, C. & Sanchez del Rio, M. (2014). *J. Synchrotron Rad.* **21**, 507–517.
- Zhang, L., Barrett, R., Friedrich, K., Glatzel, P., Mairs, T., Marion, P., Monaco, G., Morawe, C. & Weng, T. (2013). *J. Phys. Conf. Ser.* **425**, 052029.